Precise Traveling Wave Based Transmission Line Fault Location Method Using Single-Ended Data

O.D. Naidu, *Senior Member, IEEE*, and Ashok Kumar Pradhan, *Senior Member, IEEE*

***Abstract*—In this paper, an accurate single-ended traveling wave-based fault location method is proposed for transmission lines with the inputs as the first three arrival times of traveling wave wavefronts and wave velocity of the line. In the calculation process, two fault distances are obtained considering the fault in the first or second half segment of the line by using the first (incident) and second (reflected) wavefronts. The third wavefront is then used to determine the faulted half segment and thereby select the correct fault distance out of the two. The technique is economical, and it does not require communication. The proposed technique is verified on a 400 kV, 50 Hz, 150 km two-terminal line using EMTDC simulations with a realistic line model. The performance of the method is evaluated for different fault locations, fault inception angles, and fault resistances. The test results obtained by the proposed method are compared with a practically proven two-terminal communication-based method and are found to be accurate.**

***Index Terms*—Fault location, line fault, single-ended method, transmission lines, time of arrival, traveling-waves**

I. Introduction

FAULTS in power transmission lines occur as a consequence of bad weather conditions such as hurricanes, heavy snowfall, failure of insulators, insulation breakdown by nature, and tree fall on the overhead circuit [1]. Transient faults are self-cleared and in case of a permanent fault, the line is energized only after the service team identifies and replaces the damaged component. Fault position identification and fast restoration of a faulted transmission line are important tasks for the transmission system operators (TSOs). For this purpose, a precise fault position should be identified, otherwise, the inspection task becomes tedious and time consuming for high voltage long transmission lines. Thus, the precise fault location is very crucial information for the service staff to perform repair and restoration of the power supply. Fast restoration of power supply improves reliability, and customer satisfaction and results in a less commercial loss.

Fault location (FL) techniques are broadly classified into three categories [2]; fundamental phasor-based, traveling wave (TW) based, and artificial intelligence (AI) based techniques. Fundamental phasor-based FL methods are most commonly employed by TSOs because of ease of use, low sampling rate data requirement, and low hardware cost [3]. However, the precision of phasor-based FL algorithms [4] is influenced by the type of fault, arc resistance, impedance angles of line and source, phasor estimation technique, measurement transformer inaccuracies, current transformer (CT) saturation, power flow direction, and source to line impedance ratios (SIRs) [5]-[6]. Therefore, the phasor-based FL methods have limited performance scope.

Traveling wave-based FL methods [7] are gaining great importance to mitigate the disadvantages of power frequency-based approaches. The performance of TW based FL methods depends only on accurate detection of wavefront arrival times, sampling frequency, and time synchronization. With new developments in signal processing and data acquisition systems, TW based FL methods are potential alternatives when higher FL precision is required [7]. Two ended synchronized data-based TW fault location algorithms are presented in [7]. Two ended TW based FL method using unsynchronized data are presented in [8]-[10]. In [11], a model-free TW based FL method using unsynchronized data is proposed. A fault location method that utilizes information of the time differences of arrival of modal traveling waves asynchronously sampled in the network is proposed in [12]. Accuracy and dependability are notable attributes of two ended TW algorithms. However, a major demerit of two ended FL methods is that they may not work for faults during line energization, particularly when a remote breaker is open, and the remote current measurements are not available. The precision of the two ended algorithms [9] relies on the accuracy of time synchronization, asymmetrical processing delays introduced when using IEDs with different signal processing at each line terminal. These signal processing differences can be adjusted by manual tuning of two-ended algorithms. However, determination of the tuning parameters may require conducting practical experiments such as creating a fault at a known distance and computing the signal measurement delay. Moreover, communication-based FL methods are expensive for practical deployment.

Single-ended approaches are preferred by TSOs as an alternative to the communication-based TW methods [7]-[12] and fundamental phasor techniques [4]-[6]. In these methods, the fault location is calculated using single-ended TW information without needing any communication and GPS signals [13]-[17]. Although relatively economical and easier to deploy, these algorithms are posed with the problem of identifying the source of the second TW wavefront, i.e., whether it is reflected from the fault position or the remote impedance discontinuity point [13]-[15] of the line. This information is critical for the single-ended TW based fault location calculation.

To overcome these problems, combined impedance and TW based methods are proposed in [15]-[17]. These single-ended methods which involve impedance-based fault location to identify the faulted half segment (source of the second reflection). As mentioned earlier, the reliability of phasor or impedance-based methods depends on the accuracy of phasor estimation during the transient period, system homogeneity (X/R ratio of the source and line), fault type, fault resistance, and remote infeed [4]. A parameter-free single-ended TW based

method is proposed in [17]. In this approach also, the faulted half segment identification uses a single-ended impedance-based method and therefore has the same limitations. Additionally, the process also requires at least one reflection from the remote terminal to estimate the line length.

Artificial Intelligence (AI) based methods have been investigated in [19, 20] to identify the faulted half segment. Machine learning (ML) models can be trained using data obtained from EMTDC/PSCAD simulations [21] of various fault cases. Although AI/ML is gaining momentum in the recent researches and real-life applications, they face issues when applied to problems pertaining to power system protection and FL. Lack of abundant practical data and dependence on simulated data lead to non-coverage issues. Such methods usually take time to mature for practical deployment and offer low levels of reliability for untrained scenarios. Moreover, IED based training and deployment of such methods is not easy. From the literature survey, it is clear that there is a scope for research into precise single-ended TW based FL approaches.

In this context, this paper proposes a single-ended, *purely* TW based FL algorithm. The proposed algorithm is independent of phasor and impedance calculations; it does not involve AI/ML. It only requires simple algebraic computations using time-domain values to obtain an accurate fault location. It uses arrival times of only the first three TW wavefronts at the local IED and velocity of propagation of the transmission line. In the process, initially, two fault distances are obtained assuming that the fault to be in the first half segment (i.e. reflection from the fault position) or the second half segment of the line (i.e. reflection from the remote bus) using the first two wavefronts. The third wavefront is then applied to determine the faulted half segment which identifies the correct fault distance out of the two values.

The major contribution of this work is the identification of faulted half segment using the first three TW wavefront arrival time information at the local end only. The faulted half segment thus identified is then used to select the correct fault distance. The method provides a new approach to solve the classical single-ended fault location problem using traveling wave signals only. Thus, fault location can be calculated in real-time using the proposed method which gives scope for automatic network reconfiguration application and TW based distance protection. The method does not require communication with the remote end of the line and field experiments to tune the secondary cable delays [9] and therefore economical for practical deployment.

The rest of the paper is organized as follows: Section II outlines the details of the proposed method and provides an illustrative example. Section III presents the results of testing and validation. Section IV extends limitations and discussion towards challenges in practical implementation in special situations. Section V concludes the paper.

II. Proposed Method

The proposed algorithm is formulated using the first two TW wavefront arrival times recorded by the local IED and the wave speed of the transmission line. The issue of identifying the source of the second reflection is solved using the third TW wavefront. The method is detailed in the following subsections: (A) Traveling wave detection, (B) TW wavefront arrival time calculation, (C) the fault location formulation, (D) faulted half segment identification, and (E) illustrative example.

A. Traveling Wave Detection

With a fault, the current signal is measured and the signal is sent as an input to the IED to filter out the TWs using bandpass filter [7]. Current signals are used for capturing TWs. TWs are extracted by decomposing the phase currents into a ground and two aerial modes with reference to phase A using Clarke's transformation [22] as in (1).

$$\begin{bmatrix} I_0 \\ I_\alpha \\ I_\beta \end{bmatrix} = \frac{1}{3}\begin{bmatrix} 1 & 1 & 1 \\ 2 & -1 & -1 \\ 0 & \sqrt{3} & -\sqrt{3} \end{bmatrix}\begin{bmatrix} I_a \\ I_b \\ I_c \end{bmatrix} \quad (1)$$

where, I_0 is the ground mode signal and I_α, I_β are the aerial mode signals. The ground mode signal has more attenuation [12] than the aerial mode signals, due to more losses in the earth. The alpha mode signal is suitable for analyzing phase to ground faults and beta mode signal for the phase to phase faults [7]. In this work, the maximum of TW amplitude between alpha and beta signal is used for fault location analysis. The process of extraction of the TWs is shown in Fig.1. and the result of traveling wave detection is provided in subsection E.

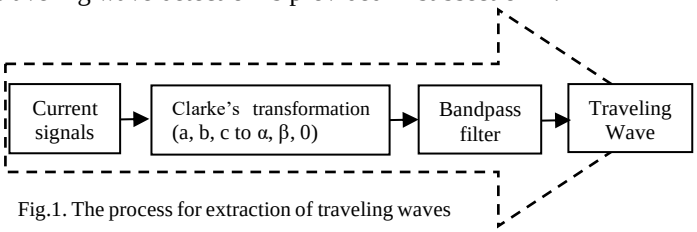

Fig.1. The process for extraction of traveling waves

B. Traveling Wave Wavefront Arrival Time Calculation

TW wavefront arrival time estimation is very important for the fault distance calculation. The TW wavefront arrival time is estimated using "leading-edge tracking" methods [23] and implemented this technique in a commericially available two-ended TW based FL method [7]. The various steps for estimating the TW wavefront arrival time used in this work are described in Fig.2. It overcomes adverse effects of signal noises and allows for more precise TW wavefronts arrival time estimation using interpolation. The squared TW signal is passed to an input to the smoother. The smoother will reduce the waveform distortions (shown within circles marked in Fig.2(b)) and thereby avoid any false zero-crossing due to noise. The finite sampling rate causes a time-quantization error in finding the exact TW time of arrival. To improve the time accuracy, the parabola-based interpolation method is applied to improve the precision of the TW wavefront arrival time calculation. This method selects three samples before and after the wavefront near to maximum value to estimate the TW time of arrival. Parabola best fit interpolation technique gives better results as compared to conventional tangent or slope based methods. This method is robust and achieved better than 0.5 μs accuracy for 1MHz sampling frequency. This method is used in commercially available FL technique described in [7].

This article has been accepted for publication in a future issue of this journal, but has not been fully edited. Content may change prior to final publication. Citation information: DOI 10.1109/TII.2020.3027584, IEEE Transactions on Industrial Informatics

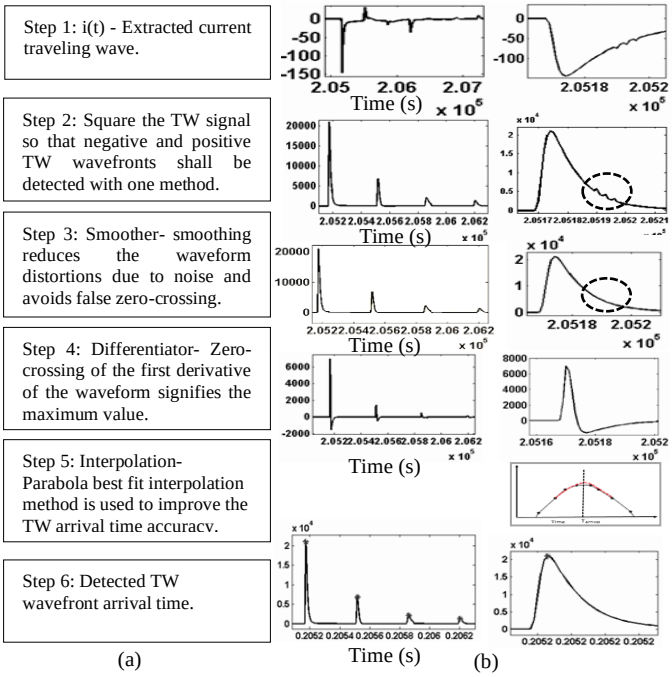

Fig.2. TW arrival time calculation (a) steps (b) wave shape for each step

C. *Single-Ended Fault Location Formulation*

Let us consider a transmission line connected between two buses A and B as shown in Fig.3. The fault locator is placed at Bus A. Now we consider two scenarios of fault location (i) fault in the first half segment (between Bus A and mid-point of the line), (ii) fault in the second half segment (beyond the midpoint). The time-space diagram presented in Fig.3 corresponding to a fault in the first half segment of the line. It is seen that in this case, both first and second TW wavefronts recorded at Bus A arrive from the fault point.

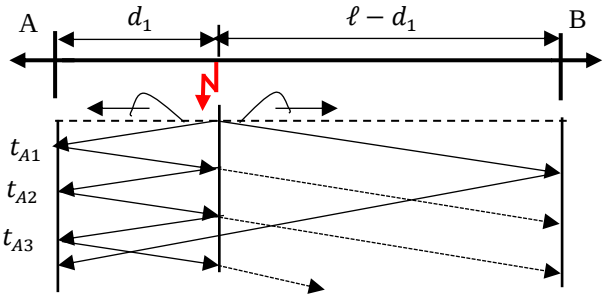

Fig. 3. Time-space diagram showing incident and reflected TWs for a fault in first half segment of the line from Bus A

From the diagram of Fig.3, we can write,

$$t_{A1} = t_{A0} + \frac{d_1}{V} \quad (2)$$

$$t_{A2} = t_{A0} + \frac{3d_1}{V} \quad (3)$$

where, d_1 = fault distance from Bus A for a fault in the first half segment; t_{A0}= fault inception time as recorded by the fault locator; t_{A1} and t_{A2}= first and second TW wavefront arrival time measured by fault locator at Bus A; V =propagation velocity of the line. Solving (2) and (3) for FL, we get,

$$d_1 = (t_{A2} - t_{A1})\frac{V}{2} \quad (4)$$

Now, let us consider fault in the second half segment of the line, lattice diagram of which is shown in Fig.4. From the figure, we can observe that the first TW incident wavefront arrives from the fault position while the second one is a reflection from Bus B.

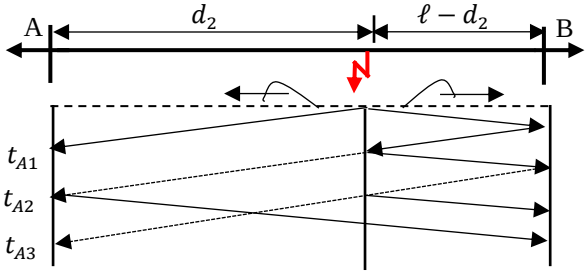

Fig. 4. Time-space diagram for fault in second half of the line from A

From the diagram of Fig.4, we can write,

$$t_{A1} = t_{A0} + \frac{d_2}{V} \quad (5)$$

$$t_{A2} = t_{A0} + \frac{2\ell - d_2}{V} \quad (6)$$

where, d_2 = fault distance from Bus A for a fault in the second half segment of the line; Solving (5) and (6), fault location is obtained as in (7) for a fault in the second half segment of the transmission line,

$$d_2 = \ell - (t_{A2} - t_{A1})\frac{V}{2} \quad (7)$$

Two fault distances d_1 and d_2 are calculated using (4) and (7) assuming the fault to be located in the first and the second half segment respectively. In order to determine the correct fault location out of these two, we need to identify the faulted half segment. A novel faulted half segment identification technique is developed which is described in the next subsection.

D. *Proposed Faulted Half Segment Identification*

In this section, we describe the proposed method for faulted half segment identification (FSI). The problem is solved by comparing the measured (actual) third TW wave arrival time with the corresponding calculated time. For the detailed description, we consider two possible scenarios.

***Case 1*: Fault in the first half segment of the line**. A challenge, in this case is the identification of the total distance traveled by the third TW wavefront before it reaches to the Bus A. From the time-space diagram of Fig.3, for a fault in the first half segment, we can write,

$$t_{A3} = t_{0A} + \frac{5d_1}{V} \quad (8)$$

If a fault is in the first half segment of the line, from (8) the distance covered by the third TW reflection is $5d_1$. However, this may not be true for all the fault cases in the first half segment of the line. For a fault that is in the first half segment of the line, the third TW wavefront seen at Bus A can be due to a reflection from the fault position or the remote Bus B. An example case for the 150 km line is presented in Fig.5 and Fig.6 to explain this situation. Fig. 5 (a). shows the time-space diagram for a fault in the first half segment at 25 km from Bus A where the fault locator is placed. As observed from the Fig.5 (a), the first reflection (t_{A1}) corresponds to 25 km. The second reflection (t_{A2}) is from the fault point corresponds to 75 km. The third reflection (t_{A3}) is from the fault point corresponds to ($5d_1$) 125 km, whereas the reflection from Bus B corresponds to (2ℓ-d_1) 275 km. Thus, in this case the distance traveled by the third wavefront is equal to $5d_1$.

This article has been accepted for publication in a future issue of this journal, but has not been fully edited. Content may change prior to final publication. Citation information: DOI 10.1109/TII.2020.3027584, IEEE Transactions on Industrial Informatics

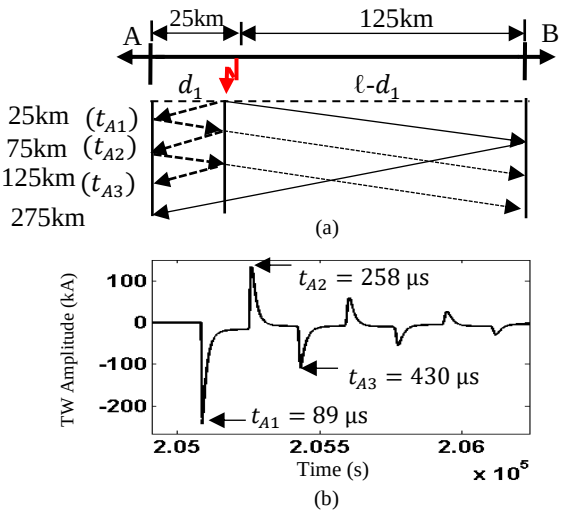

Fig. 5. (a) Time-space diagram for fault at 25km from Bus A and (b) three TW wavefront arrival recorded by fault locator at Bus A

Fig.6(a) shows the time-space diagram for a fault at 70 km of a 150-km transmission line case. As observed from Fig.6(a), the first reflection (t_{A1}) corresponds to 70 km. The second reflection of TW at (t_{A2}) which is from the fault point corresponds to 210 km. The third TW reflection is from Bus B and corresponds to (2 ℓ -d_1) 230 km, while the third reflection

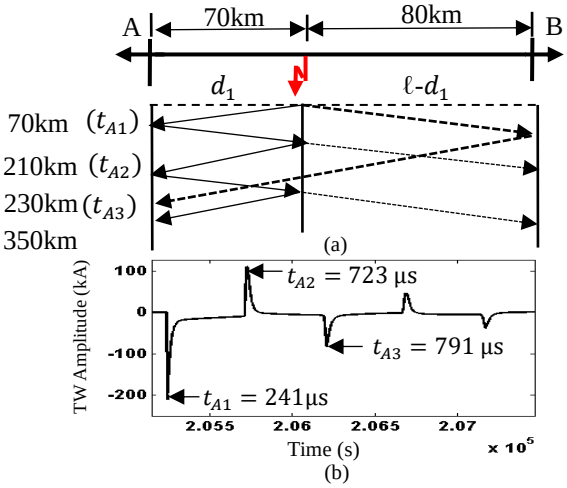

Fig. 6. (a) Time-space diagram for fault at 70km from Bus A and (b) three TW wavefront arrival time recorded by fault locator at Bus A

from the fault point corresponds to ($5d_1$) 350 km. Thus, even though the fault is in the first half segment of the line, the third TW reflection, in this case, is from Bus B, and the distance traveled by it is equal to 2 ℓ -d_1.

Therefore, from Fig.6(a), for a fault in the first half segment, we can write,

$$t_{A3} = t_{0A} + \frac{2\ell - d_1}{V} \quad (9)$$

From the above discussions we can conclude that the for a fault in the first half segment, the third TW wavefront always travels a distance which is the minimum of ($5d_1$) and (2 ℓ -d_1). Using the calculated distance (d_1) as per (4), a distance corresponding to the third TW wavefront arrival time is obtained as shown in (10),

$$\text{d\_3}^{rd}\text{ wavefront\_first} = \text{minimum } (5d_1, (2\ell - d_1)) \quad (10)$$

The third TW wavefront arrival time is then calculated as shown below in (11),

$$t_{A3\_First} = \frac{\text{d\_3rd wavefront\_first}}{V} \quad (11)$$

***Case 2*: Fault in the second half segment of the line**. Fig.7 (a) shows the time-space diagram for a fault at 125 km from Bus A of a 150-km transmission line case. As noticed, the first reflection (t_{A1}) corresponds to 125 km. The second reflection of TW at (t_{A2}) which is from Bus B corresponds to 175 km and the third which is also from Bus B corresponds to ($4\ell - 3d_2$) 225 km. Thus, for a fault in the second half segment of the line, the third TW reflection is from Bus B. From Fig.7 (a), we can write,

$$t_{A3} = t_{0A} + \frac{4\ell - 3d_2}{V} \quad (12)$$

As analyzed in Case1, using the calculated distance (d_2) as per (7), a distance corresponding to the third TW wavefront arrival time is obtained as shown in (13)

$$\text{d\_3}^{rd}\text{ wavefront\_second} = \text{minimum } (4\ell - 3d_2, 5d_2) \quad (13)$$

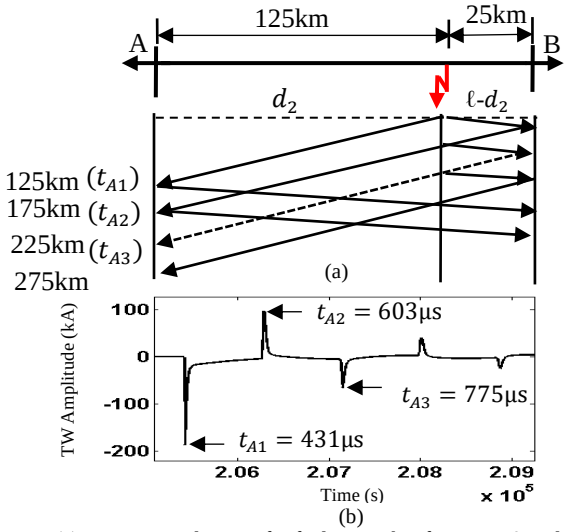

Fig. 7. (a) Time-space diagram for fault at 125km from Bus A and (b) three TW wavefronts recorded by fault locator at Bus A

The third TW wavefront arrival time is calculated as in (14),

$$t_{A3\_second} = \frac{\text{d\_3rd wavefront\_second}}{V} \quad (14)$$

The two values of t_{A3} calculated using (11) and (14) are compared with the actual third wavefront arrival time recorded by the fault locator at Bus A. The faulted half segment is then identified as that half segment for which the calculated third wavefront arrival time is closer to the recorded value. A comparison threshold (ϵ) of 2µs can be used for 1 MHz sampling rate.

***Special case:* Fault at the midpoint of the line.** If the calculated distances d_1 and d_2 (as per (4) and (7) respectively) are close to $\ell/2$ or the absolute difference between d_1 and d_2 is less than the threshold (ϵ) of 600meters, then the fault is determined to be at the midpoint of the line. Final fault location is then recorded as the mean of (d_1 and d_2). The steps of the proposed algorithm are depicted in Fig.8.

This article has been accepted for publication in a future issue of this journal, but has not been fully edited. Content may change prior to final publication. Citation information: DOI 10.1109/TII.2020.3027584, IEEE Transactions on Industrial Informatics

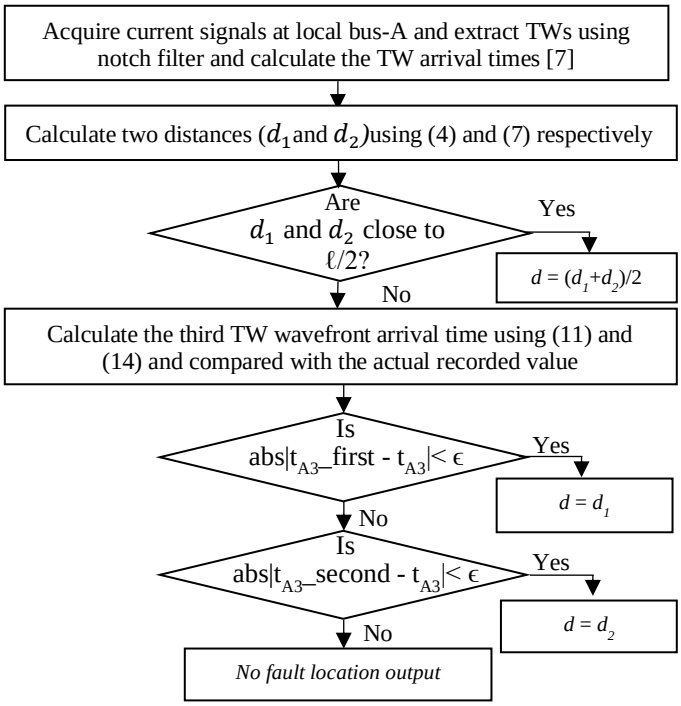

Fig. 8. Flowchart for proposed single ended fault location technique

In this work, we used two thresholds; (ϵ) and (ε). Thresholds (ϵ) and (ε) are defined 2 μs and 600 meters respectively for 1MHz sampling adopted in the work. The values are chosen based on the accuracy requirement of the fault location which in turn depends on sampling frequency. For example, the accuracy that can be achieved with 1MHz sampling is ~ ±300 meters (i.e. theoretically maximum possible error =propagation velocity x signal sampling rate). This means a 1 μs (sampling interval) error in TW peak arrival time estimation can lead to an error of 300 meters assuming wave speed be approximately light speed. Considering a margin of two sample time error in TW arrival estimation, we have chosen the values of the thresholds as 2μs and 600 meters respectively.

E. Illustrative Example

A 400 kV, 50 Hz system consisting of a transmission line of 150 km is modeled in PSCAD/EMTDC simulation tool for testing the method. The system is similar to that shown in Fig. 3 with the addition of two sources at each terminal. This two-terminal system is named as Test System 1 for reference in the rest of the paper. The transmission line tower configuration is shown in Fig.13 in Appendix. A current transformer (CT) model [24] is included in the simulation to measure the current signals. The source details are provided in Table VIII in the Appendix. The fault locator is placed at Bus A. The percentage error of FL is calculated using (15)

$$\%\text{Error} = \left|\frac{\text{Actual FL}-\text{Calculated FL}}{\text{The total length of the line}}\right| \text{x } 100 \qquad (15)$$

The current signals are measured at local IED at a sampling frequency of 1MHz. TWs are filtered using a bandpass [7] filter. Fixed wave speed is considered in this work. The wave speed can be obtained using line parameters (inductance and capacitance). Another practical approach to obtain the wave speed is to capture it from any switching event. For example, with one end of the line open, the line from the remote end is energized. The TW wavefront arrival time at the local (IED) end is captured and then the wave speed is calculated based on the known distance (line length) traveled. This method is accurate and commonly employed for the practical deployment of TW-based FL [7]. The wave speed used for the simulated line is 2.90398525e+08 m/s. For the illustration, we consider a fault at 50km from bus A. The fault resistance and fault inception angle considered are 50Ω and 60^0 respectively for the simulated case. The corresponding three-phase currents and the alpha mode signal are shown in Fig.9(a) and 9(b) respectively. The high-frequency transient (traveling waves) component is marked in a dotted circle in Fig.9 (a) and (b). Note that the process described in Fig.1 is used to obtaining the aerial (alpha) mode signal (Fig.9(b)) from which the TWs are extracted as shown in Fig.9(c). The TW wavefront arrival times are calculated using the process shown in Fig.2. and they are marked in Fig.9(c) for the case.

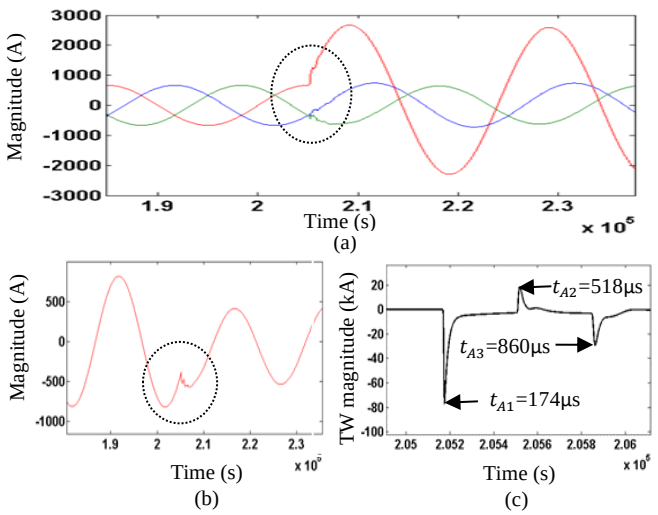

Fig. 9. Phase A-to-ground fault at 50km from bus A of the line (a) three-phase currents (b) Alpha component of the current signal and (c) traveling waves

The fault distances d_1 and d_2 calculated using (4) and (7) are 49.914km and 100.051 km respectively. The third wavefront arrival time recorded at Bus A is 860μs. Assuming that the fault is in the first half segment, the minimum distance traveled by the third reflection calculated using (10) is 249.570 km and the calculated third wavefront arrival time using (11) is 859μs. Assuming fault in the second half segment, the minimum distance traveled by the third reflection calculated using (13) is 299.847km and the calculated third wavefront arrival time using (14) is 1032μs. It is clear that the calculated third wavefront arrival time for fault in the first half segment is closer to the actual arrival time of 860 μs (difference of only 1 μs), which indicates that the fault is in the first half segment and therefore, the correct fault location is 49.914km. Four fault locations covering all possible faulted segments are simulated on Test System 1 to prove the accuracy of the method. The results are listed in Table I. It is observed from Table I, that the maximum error of FL is 0.11% (170 m) for a 150-km transmission line. Note that in the case where the fault is located

at the mid-point of the line (75 km), the algorithm identifies the same and the fault location becomes the average of d_1 and d_2.

TABLE I
TEST RESULTS FOR THE PROPOSED FAULT LOCATION METHOD

Test Case/ Parameter	FL at 25 km from Bus A	FL at 70 km from Bus A	FL at 75 km from Bus A	FL at 125 km from Bus A
t_{A1} (μS)	89	241	259	431
t_{A2} (μS)	258	723	772	603
t_{A3} (μS)	**430**	**791**	783	**775**
d_1 (km)	**24.83**	**69.98**	**74.82**	25.11
d_2 (km)	125.17	80.01	**75.18**	**124.89**
d_1_3rd wavefront (km)	124.15	230.02	NA	125.55
d_2_3rd wavefront (km)	224.49	359.97	NA	225.33
t_{A3}_using (d_1) (μs)	**431**	**792**	NA	89
t_{A3}_using (d_2) (μs)	773	1239	NA	**776**
FL (d) (km)	**24.83**	**69.98**	**75**	**124.89**
FL Error (m)	170	20	0	110
FL Error (%)	**0.11**	**0.01**	**0**	**0.07**

III. RESULTS AND DISCUSSIONS

In this section, we provide the results of testing and validation of the proposed method for FL. Specifically, we carried out the following studies: (A) comparison with a practically proven communication-based method, (B) testing the method for fault inception at near voltage zero crossing, (C) testing the method under the influence of signal noise and sampling frequency, (D) performance of the method under special cases, (E) extensive testing of the method with two test systems. Following this, we extend a discussion on the challenges in practical implementation under certain special situations

A. Comparison with Communication-Based Method

Here we compare (Table II) the proposed method with a practically established communication-based method [7]. The comparison considers the phase-to-ground, phase-to-phase, and phase-to-phase-to-ground faults with an arc resistance of 100, 10, and 50Ω respectively. The fault inception angles (FIA) of 0^0, 60^0, 90^0, and 150^0 and different FLs 5, 75, and 145 km from Bus A of Test System 1 are considered for this study. Results from Table II confirm that the technique can locate the fault very precisely for different fault situations. In comparison with the method in [7], the performance of the proposed method is found to be at par, as second and third wavefronts are available in all these situations. Note that with the proposed method the error for the cases where the fault is at the midpoint of the line is 0% as in these cases the final FL is calculated as the mean of d_1 and d_2.

It is important to note that Table II shows the accuracies based on results obtained using ideal simulations without accounting for noise and errors in measurements as will be the case in any practical implementation. The comparable accuracy can be attributed to the identical underlying principles of both the approaches with the traveling waves. In fact, in a practical implementation double-ended methods may yield better results as they typically require only the first TW wavefront arrival time unlike the proposed single-ended method which requires arrival times for the first three TW wavefronts. Capturing the third TW wavefront accurately under noisy conditions can be challenging for certain situations (discussed in section IV). However, it is worth pointing out that the proposed method is advantageous in cases where two-ended time-synchronized data and reliable communication are not available.

TABLE II
COMPARISON OF THE PROPOSED METHOD WITH THE COMMUNICATION BASED METHOD [7]

Test cases	Two ended method [7]			Proposed method	
	FIA (deg)	FL (d) (km)	Error (%)	FL(d) (km)	Error (%)
A-g fault, Rf 100 Ω and FL 5km	0	4.81	0.12	5.2	0.13
	60	4.81	0.12	5.2	0.13
	90	4.81	0.12	5.2	0.13
	150	4.81	0.12	5.2	0.13
AB fault, Rf 10 Ω and FL 75km	0	74.8	0.13	75.0	0.00
	60	74.8	0.13	75.0	0.00
	90	74.8	0.13	75.0	0.00
	150	74.8	0.13	75.0	0.00
BC-g fault, Rf 50 Ω and FL 145km	0	145.18	0.11	145.19	0.12
	60	145.18	0.11	145.19	0.12
	90	145.18	0.11	145.19	0.12
	150	145.18	0.11	145.19	0.12

B. Evaluation Study for Fault Inception at Near Voltage Zero-Crossing Point

Faults occurring at near voltage zero-crossing pose the problem of subdued post fault transients in the current. Therefore, it is important to test FL algorithms under such scenarios. Phase-to-ground and phase-to-phase faults with fault inception at voltage zero-crossing are considered for the study. Also, different fault resistances of 0.01, 50 Ω for phase-to-ground faults, and 0.01, 25 Ω for phase-to-phase faults are used for simulations. Two fault locations, one at 50 and other at 100 km from Bus A of Test System 1 are considered and the results are presented in Table III. It is found that the proposed method can identify the faulted half segment and location accurately in these conditions.

TABLE III
EVALUATION STUDY FOR FAULT INCEPTION AT VOLTAGE ZERO CROSSING

Fault type	R_F (Ω)	Actual FL (km)	Calculated FL (km)	Error (%)
A-g	0.01	50	49.978	0.01
	0.01	100	100.043	0.02
	50.00	50	49.978	0.01
	50.00	100	100.043	0.02
AB	0.01	50	49.966	0.02
	0.01	100	100.067	0.04
	25.00	50	49.966	0.02
	25.00	100	100.067	0.04

C. Study on Signal Noise and Sampling Frequency

Noise in the measured current signals tends to adversely affect the performance of fault location algorithms. In this study, we verified the proposed technique with different levels of measurement noise under varying sampling rates. The results

are presented in Table IV. The precision of TW based FL depends on the TW wavefront detection and time of arrival calculation. In the proposed technique, an advanced interpolation algorithm [7] is used for TW wavefront arrival time calculation. This interpolation technique improves the FL precision even with the low sampling rate and signal noise. The results reveal that noise has no significant influence on FL precision. The maximum FL error is found to be 1.14% of the sampling rate of 1MHz.

TABLE IV
STUDY OF SIGNAL NOISE AND SAMPLING RATE ON THE FL PRECISION

Sampling Frequency	Percentage of FL Error							
	No noise		0.5% Noise		1% Noise		2% Noise	
	Avg.	Max.	Avg.	Max.	Avg.	Max.	Avg.	Max.
250 kHz	0.47	1.19	0.89	1.38	0.67	1.72	1.17	2.01
500kHz	0.27	0.48	0.31	0.51	0.31	0.57	0.35	1.47
1MHz	0.07	0.13	0.08	0.17	0.10	0.19	0.68	1.14
2MHz	0.05	0.11	0.05	0.12	0.06	0.13	0.61	1.17

It is also observed that errors are appreciable only when the method is implemented with lower sampling rates, and the noise level is more than 1%. This is because the method is unable to calculate accurate TW arrival time for high resistance ground fault during low sampling frequency. It can thus be concluded that the proposed technique is accurate and can achieve the utility required FL accuracy of two tower spans (280-320m) distance using a 1MHz sampling rate.

D. Study on Impact of Adjacent Short Transmission Lines

When the monitored line (i.e. the line on which the fault locator is placed) is adjacent to short lines, multiple reflections may be received at the fault locator. This makes identification of the source of the traveling waves related to the monitored line is difficult. This issue is resolved by using TW topology stamp [17] information. In this approach, it is to identify and eliminate the reflections and refractions from the remote stations, and other impedance discontinuity points using reference TW wavefront arrival times. The reference wavefront arrival times can be captured during line energization [17] with the remote breaker of the protected line open. The reference wave arrival time provides information about the line topology and adjacent junctions, tap, and station reflections. By using the reference wave arrival times along with the wave arrival times captured during an internal fault, the proposed method can locate the fault accurately. This approach does not require any directional information and it works based only on current traveling wave information [17]. The reference topology stamp may change with changes in source network topology (addition or removal of the lines) and therefore it needs to be updated. A different test system is considered to validate the proposed method with multiple adjacent lines to the monitored line as shown in Fig.10. This test system is adapted from [25] to which one extra short line (A-E) of length 30 km on Bus A is considered to study the effect adjacent short lines. This system named as Test System 2 is modeled with frequency-dependent line models using PSCAD/EMTDC tool and various fault scenarios are simulated.

We have used the network topology stamp-based method [17] to eliminate the extra reflections. The fault location results for the simulated cases are presented in Table V.

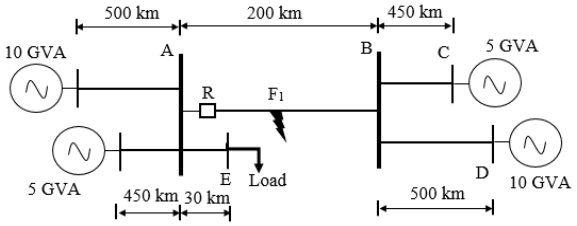

Fig. 10. 400-kV transmission network with adjacent short lines

The results in Table V confirm that the proposed method is able to sort out the TW reflections/refractions from short adjacent lines successfully using reference TW arrival times (network topology stamp) [17] and locate the faults precisely.

TABLE V
EVALUATION STUDY ON THE EFFECT OF ADJACENT SHORT LINES

Fault type	R_F (Ω)	Actual FL (km)	Calculated FL (km)	Error (%)
A-g	50.00	50	49.914	0.04
	50.00	150	150.164	0.08
AB	25.00	50	49.914	0.04
	25.00	150	150.164	0.08

E. Results from Extensive Studies

This section provides results for Test System 1 and Test System 2 for various fault conditions. The summary of considered fault scenarios for Test System 1 is tabulated in Table IX in the Appendix. Table VI confirms that the proposed technique is capable of calculating the fault location accurately, with average and maximum errors of 0.03% and 0.13% respectively for Test System 1. The simulation conditions for Test System 2 are tabulated in Table X. As shown in Table VI, the average and maximum errors are 0.04% and 0.16% respectively for Test System 2.

TABLE VI
FAULT LOCATION RESULTS IN SUMMARY FROM EXTENSIVE STUDIES

Test system	No. of studied test conditions	Average Error (%)	Maximum Error (%)
1	896	0.03	0.13
2	360	0.04	0.16

IV. LIMITATIONS AND DISCUSSION

The following special situations and limitations may arise during the practical deployment of the proposed method for which associated studies are also carried out (A) the monitoring line is connected to another adjacent line with exactly the same characteristic impedance, (B) high impedance fault on a long transmission line and fault inception at near voltage zero crossing, (C) noise and sampling rate influence on FL accuracy for close-in faults and (D) monitoring line be grounded through a larger resistance. The impact and recommended solutions for each special situation are discussed in the following subsections.

This article has been accepted for publication in a future issue of this journal, but has not been fully edited. Content may change prior to final publication. Citation information: DOI 10.1109/TII.2020.3027584, IEEE Transactions on Industrial Informatics

A. The Monitored Line is Connected to Adjacent Line with Exactly Same Characteristic Impedance

One special situation that may happen in a transmission system is that the monitored line is connected to another line with *exactly* the same characteristic impedance. The following two configurations are considered to explain the validity of the proposed method under these special scenarios.

Configuration 1: Let us consider the monitored line of length ℓ_1 connected with a line of length ℓ_2 at its remote terminal as shown in Fig. 11(a). Both the lines are assumed to have equal characteristic impedances. Two cases are possible in this situation:

Case 1: An element of discontinuity such as load is connected at the interconnection point, i.e., Bus B. This type of configuration is common in practice. In this case, the fault locator at Bus A will locate the fault for the transmission line of length ℓ_1 using the proposed method without any modification, as there will be TW reflections from Bus B due to the connected load.

Case 2: Interconnecting Bus B does not have any load or other element connected to it. In this case, we need to consider the new equivalent line length of ℓ ($=\ell_1+\ell_2$). The fault locator at Bus A will then locate the fault for length ℓ using the proposed method, as TW reflections will come from Bus C. This means that in such a case, the protected line length should be considered equal to the sum of the lengths of the two lines.

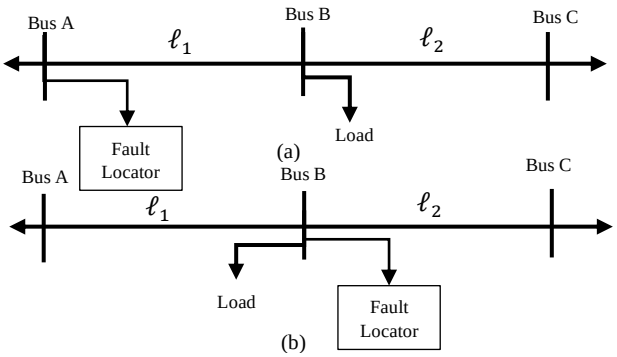

Fig.11. Line with same characteristic impedance is connected at (a) remote terminal and (b) fault locator terminal

Configuration 2: Let us consider the monitored line of length ℓ_1 connected with a line of length ℓ_2 at its monitored terminal as shown in Fig. 11(b). Both the lines are assumed to have equal characteristic impedances. The same two cases are possible in this situation as well. As in the previous configuration, the proposed method shall work well for Case1.

But in Case 2, the proposed method will not work, as there will be no reflected traveling waves captured at fault locator at Bus B. This is indeed a common limitation for single-ended fault location methods. However, in this situation, the fault locator should be placed at bus A to locate the faults on a new equivalent line of length ($\ell_1+\ell_2$).

It is worth noting that the case of two adjacent lines with *exactly* the same characteristic impedance and without any impedance discontinuity at the interconnection is rare in any interconnected high voltage transmission network. Transmission lines are typically connected through elements such as a breaker, isolator, surge arrestors, and loads. The interconnecting substation may also have loads, shunt reactors, etc. which can offer impedance mismatch, and hence TW reflections will be available for FL analysis.

B. High Resistance Faults on Long Transmission Lines

The impact of the proposed method for high resistance faults on a long transmission line is analyzed in this section. The third TW wavefront may be attenuated for faults in the middle of the long transmission line with very high fault resistance especially for fault inception at near voltage zero crossing. In this case, the detection of the third wavefront may not be guaranteed always. Let us consider three fault cases on a long line of length 400km for the analysis. The rest of the simulation parameters are the same as used in Test system 1.

Case 1: Phase A-to-ground fault at 150km of the line with fault resistance of 50Ω and FIA at near voltage zero crossing.

Case 2: Phase A-to-ground fault at 150km of the line with fault resistance of 200Ω and FIA is 90^0.

Case 3: Phase A-to-ground fault at 150km of the line with fault resistance of 200Ω and FIA at near voltage zero crossing.

The total distance traveled by the third TW wavefront is 750km (5x150) for the above three cases. The recorded traveling waves are as shown in Fig.12. From the figure, it is clear that the proposed method can locate faults for Case 1 and 2, as the third wavefront can be measured even for the worst-case scenarios. For Case 3, the proposed method may not work as the third wavefront is highly attenuated due to high fault resistance and fault inception at near voltage zero crossing. It is therefore concluded that the performance of the proposed method can be limited for very high impedance faults with fault inception at near voltage zero crossing, especially for long lines. In this context, it is important to note that majority of the faults in transmission lines are insulator failures. Such failures generally occur at the rising edge (fault inception at around 60^0) of the voltage waveform and fault resistance may be less than 50 Ω for practical cases. A significant third TW wavefront will be available in such conditions and the method will work as expected. The method is tested for fault resistance (R_F) of 50Ω and various FIAs for a long line of length 400km. The results

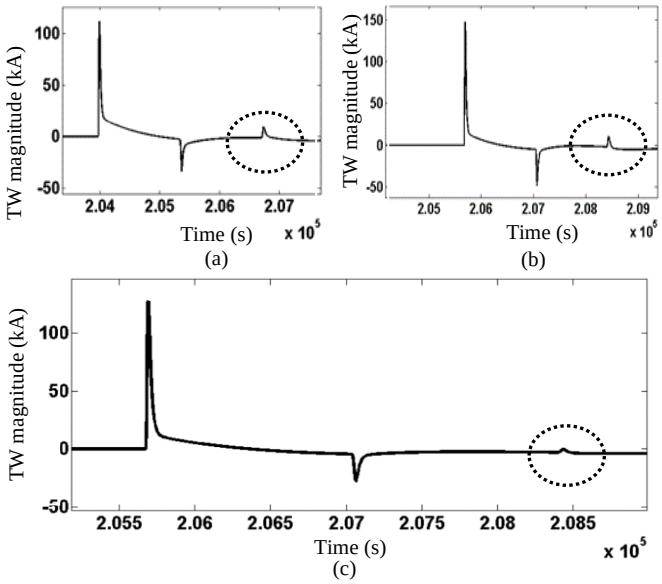

Fig.12. Phase A-to-ground fault at 150km from fault locator of 400km long line (a) Case 1 (b) Case 2 and (c) Case 3

are listed in Table VII which shows that the proposed method is able to locate the faults accurately for long transmission lines.

TABLE VII
RESULTS FOR HIGH RESISTANCE FAULTS ON A LONG TRANSMISSION LINE

Fault case	FIA (deg)	Actual FL (km)	Calculated FL (km)	FL Error (%)
A-g fault at 150km and R_F of 50Ω	0	150	149.802	0.04
	90	150	149.802	0.04
	135	150	149.802	0.04
	180	150	149.802	0.04
A-g fault at 300km and R_F of 50Ω	0	300	300.268	0.06
	90	300	300.268	0.06
	135	300	300.268	0.06
	180	300	300.268	0.06

C. Noise and Sampling Rate Influence on FL Accuracy for Close-in Faults

The FL errors are appreciable for close-in faults when the proposed single-ended method is implemented with lower sampling rates (500kHz or below), and when the noise level is more than 1%. This is because the method is unable to detect the second and third TW arrival times accurately for the close-in fault at a low sampling rate with higher noise. In this situation, double-ended methods may be more robust and reliable as it requires only first TW arrival times which can be captured accurately. The minimum recommended sampling rate for the proposed method is 1MHz to achieve the accuracy of two tower span distance.

D. The Monitored Line is Grounded Through a Large Resistance

The impact of the monitored line being grounded through a larger resistance is analyzed. The system grounding will not affect the accuracy of the TW based methods [26]-[27], as the accuracy of these methods depends only on the TW wave arrival times. The traveling waves being generated during fault are independent of the neutral grounding method. Typically, transmission lines are effectively grounded through the wye winding of transformers and autotransformers [28]. In these cases, the method will work as expected, as TW reflection/refractions are generated due to a change in impedance at transformer or ground resistance.

V. CONCLUSION

In this work, TW based FL technique for a transmission line is proposed using single-ended data. The first three TW wavefront arrival times and wave speed of the line are the only inputs to the fault locator. Two fault locations are calculated initially by assuming the fault in the first half segment and the second half segment of the line respectively. An accurate faulted half segment identification technique is proposed using the third TW wavefront. The faulted segment thus determined is used thereby to select the correct fault distance out of the two values. The proposed algorithm is assessed using PSCAD/EMTDC simulation study for two test systems. Test results reveal that performance of the method is accurate for different FLs, type of faults, fault resistance, and fault inception angles. The performance of the method is comparable to a practically proven two ended (communication-based) method. Simulation studies also reveal that it is possible to achieve FL precision of ± 300 m using 1MHz sampling frequency. The performance and usability of the method under special situations such as adjacent lines which are short or have the same characteristic impedances are also investigated.

The technique can be implemented in IEDs with a minimum sampling rate of 1MHz to achieve the FL precision of two tower span distance (~320m). This technique does not require any communication infrastructure and field experiments to compensate for the processing delays introduced by various components of IEDs and measurement systems. Thus, it is cost-effective and suitable for practical deployment.

Importantly, the method facilitates fault location determination in near real-time which can be used for automatic network reconfiguration application in control centers or fault location as a cloud-based service. The proposed method can also be explored for application to distance element for TW-based distance protection.

APPENDIX

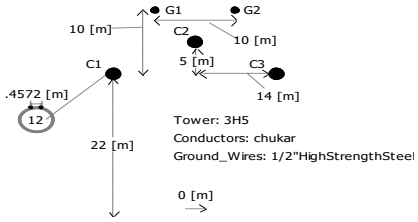

Fig. 13. Tower configuration for the simulated transmission line

TABLE VIII
SOURCE PARAMETERS CONSIDERED FOR THE SIMULATION STUDY

Source	Positive sequence		Zero sequence	
	R (Ω)	L (H)	R (Ω)	L (H)
A	3.135	0.094	2.437	0.063
B	3.051	0.110	3.219	0.079

TABLE IX
FAULT CASES CONSIDERED FOR TEST SYSTEM 1

Test cases	Test conditions
FL (km)	5, 10, 25, 50, 75, 95, 125, and 145
Type of fault	a-g, a-b, a-b-g, and a-b-c-g
FIA (degree)	0, 30, 60, 120, 135, 150, and 180
Arc resistance (Ω)	0.01, 10, 50, and 100

TABLE X
FAULT CASES CONSIDERED FOR TEST SYSTEM 2

Test cases	Test conditions
FL (km)	10, 60, 100, 140 and 190
Type of fault	a-g, a-b, a-b-g, and a-b-c-g
FIA (degree)	0, 60, 90, 120, 135, and 150
Arc resistance (Ω)	0.01, 10, and 50

REFERENCES

[1] M. M. Saha, J. Izykowski, and E. Rosolowski, *Fault Location on Power Networks*, London, U.K.: Springer, 2010, Ed.

[2] "IEEE Guide for Determining Fault Location on AC Transmission and Distribution Lines", *IEEE Standard C37.114*, 2004.

[3] J. Izykowski, E. Rosolowski, P. Balcerek, M. Fulczyk, and M. Saha, "Accurate noniterative fault location algorithm utilizing two-end un-synchronized measurements," *IEEE Trans. Power Del*., vol. 25, no. 1, pp. 72–80, Jan. 2010.

[4] S. Das, S. Santoso, A. Gaikwad, and M. Patel, "Impedance-based fault location in transmission networks: *Theory and application*," *IEEE Access*, Vol. 2, pp. 537–557, 2014.

[5] E.O. Schweitzer, III, "A review of impedance-based fault locating experience," presented at the *14th annu. Iowa-Nebraska Syst. Protect. Seminar*, Omaha, NE, USA, Oct.1990.

[6] A. L. Dalcastagne and S. Zimath, "A study about the sources of error of impedance-based fault location methods," presented at the *IEEE/PES Transm. Distrib. Conf. Expo*.: Latin Amer., Bogota, Colombia, 2008.

[7] E. O. Schweitzer, III, A. Guzmán, M. V. Mynam, V. Skendzic, B. Kasztenny, S. Marx, "Locating faults by the traveling waves they launch", *Proc. 50th Annu. Minnesota Power Syst. Conf.*, pp. 95-110, Nov. 2014.

[8] F. V. Lopes, K. M. Silva, F. B. Costa, W. L. A. Neves, D. Fernandes, "Real-time traveling wave-based fault location using two-terminal unsynchronized data" *IEEE Trans. Power Del*., vol. 30, no. 3, pp. 1067-1076, Jun. 2015.

[9] O. D. Naidu, and A. K. Pradhan, "A traveling wave-based fault location method using unsynchronized current measurements" *IEEE Trans. Power Del*., vol.34, no.2, pp.505-513, Oct.2018.

[10] F. V. Lopes, Lima. P, J. P. G. Ribeiro, Tiago. R. H, K. M. Silva, E. J. S. Leite Jr, W. L. A. Neves and G. Rocha "Practical methodology for two-terminal traveling wave-based fault location eliminating the need for line parameters and time synchronization", *IEEE Trans. Power Del.*, vol. 34, no. 6, pp. 2123-2134, Dec. 2019.

[11] F. V. Lopes, Dantas, K. M., Silva, K. M., and Costa, F. B. "Accurate two-terminal transmission line fault location using traveling waves", *IEEE Trans., on Power Delivery*, vol.33, pp.873-880, Apr.2018.

[12] R. Liang, N. Peng, L. Zhou, X. Meng, Y. Hu, Y. Shen and X. Xue "Fault Location Method in Power Network by Applying Accurate Information of Arrival Time Differences of Modal Traveling Waves," in *IEEE Trans.Ind.Inform.*, vol. 16, no. 5, pp. 3124-3132, May 2020.

[13] D. Spoor and J. G. Zhu, "Improved single-ended traveling-wave fault location algorithm based on experience with conventional substation transducers," *IEEE Trans. Power Del*., vol. 21, no. 3, pp. 1714–1720, Jul. 2006.

[14] D. J. Spoor, J. Zhu, and P. Nichols, "Single-ended traveling wave based fault location on two terminal transmission lines, *IEEE TENCON conference*, Singapore, January 2010.

[15] M. da Silva, D.V. Coury, M. Oleskovicz and E.C. Segatto , "Combined solution for fault location in three-terminal lines base on wavelet transforms," *IET Gener. Trans. and Distri.*, vol. 4, no. 1, pp. 94-103, January 2010.

[16] E. E. Ngu and K. Ramar , "A combined impedance and traveling wave based fault location method for the multi-terminal transmission line," *International Journal of Electrical Power and Energy Systems*, vol. 33, no. 10, pp. 1767-1775, December 2011.

[17] A. Guzman, B. Kasztenny, Y. Tong and M. V. Mynam, *"*Accurate and economical traveling-wave fault lacating without communications*"procedings of the 71st Annual Conference for Protective Relay Engineers*, College Station, TX, March 2018.

[18] X. Kong, Y. Xu, Z. Jiao, D. Dong, X. Yuan and S. Li, "Fault Location Technology for Power System Based on Information about the Power Internet of Things," in *IEEE Trans.Ind. Inform.*, doi:10.1109/TII.2019.2960440, *Early Access.*

[19] Tabatabaei, M. R. Mosavi, and P. Farajiparvar, "A traveling-wave fault location technique for three-terminal lines based on wavelet analysis and recurrent neural networks,' *IEEE Conf. Pub. On Smart Grid*, pp.268-272, 2013.

[20] H. Livani, C. Y. Evrenosoglu, "A machine learning and wavelet-based fault location method for hybrid transmission lines", *IEEE Trans. Smart Grid*, vol. 5, no. 1, pp. 51-59, Jan. 2014.

[21] *PSCAD/EMTDC. ver. 4.6, Manitoba HVDC Research Centre*.

[22] E. Clarke, Circuit Analysis of AC Power Systems, Symmetrical and Related Components, John Wiley & Sons, NY, 1943.

[23] F. E. Nathanson, *Radar Design Principles: Signal Processing and the Environment*, McGraw-Hill Book Co., 1969.

[24] A. Bonetti, M. V. V. S. Yalla and S. Holst, "The IEC 60255-121:2014 standard and its impact on performance specification, testing and evaluation of distance protection relays," *2016 IEEE/PES Transmission and Distribution Conference and Exposition (T&D)*, Dallas, TX, 2016, pp. 1-6.

[25] P. Jafarian and M. sanaye-Pasand, "A traveling-wave-based protection technique using wavelet/PCA analysis", *IEEE Trans.Power Del*., vol.25, no.2, pp.588-599, Apr.2010.

[26] X. Dong, J. Wang, S. Shi, B. Wang, B. Dominik and M. Redefern, "Traveling wave based single-phase-to-ground protection method for power distribution system," in *CSEE Journal of Power and Energy Systems*, vol. 1, no. 2, pp. 75-82, June 2015.

[27] X. Dong et al., "Travelling wave based single phase grounding protection for distribution system," *12th IET International Conference on Developments in Power System Protection (DPSP 2014)*, Copenhagen, 2014, pp. 1-5.

[28] D. D. Ronde, R. VanHatten and A. Wade, "Loss of effective system grounding-best practices protection challenges and solutions", *Annual Georgia Tech Protective Relaying Conference*, 2014, pp. 1-8.

OD Naidu (M'13–SM'20) received M.Tech. degree in power systems engineering from Indian Institute of Technology (IIT), Kharagpur, India, in 2008. He is pursuing Ph.D. degree in Electrical Engineering, Indian Institute of Technology, Kharagpur. He is currently working as Senior Principal Engineer, at Hitachi ABB Power Grids R&D Center, Bangalore, India. From 2012 to 2019, he was Principal Scientist, at ABB Corporate Research Center, Bangalore, India. From 2009 to 2012, he was senior power system application development engineer, at ABB GISPL, Bangalore, India. He is author of more than 30 scientific papers and patent applications. His research interests including power system protection, fault location, renewable integration and monitoring, artificial intelligence applications to power system protection and monitoring.

Ashok Kumar Pradhan (M'94–SM'10) received the Ph.D. degree in electrical engineering from Sambalpur University, Sambalpur, India, in 2001. He has been with the Department of Electrical Engineering, Indian Institute of Technology, Kharagpur, India, since 2002, where he is a Professor. He served at the Department of Electrical Engineering, Veer Surendra Sai University of Technology, Burla, India, from 1992 to 2002. His research interests include power system relaying and monitoring. Prof. Pradhan is a Fellow of the Indian National Academy of Engineering, India, and Fellow of National Academy of Sciences, India.